P2

A Versatile Finite Volume Simulator for the Analysis of Electronic Properties of Nanostructures

Z. Stanojević*, M. Karner†, K. Schnass†, C. Kernstock†, O. Baumgartner*, and H. Kosina*

* Institute for Microelectronics, TU Wien, Gußhausstraße 27-29, Vienna, Austria
e-mail: (stanojevic|baumgartner|kosina)@iue.tuwien.ac.at

† Global TCAD Solutions, Graumanngasse 7, Vienna, Austria
e-mail: (m.karner|c.kernstock)@globaltcadsolutions.com, klaus.schnass@student.tuwien.ac.at

***Abstract*—We present a novel semantic approach to modeling and simulation of nanoelectronic devices. The approach is based on a finite volume spatial discretization scheme. The scheme was adapted to accurately treat material anisotropy. It is thus capable of capturing orientation and strain effects both of which are prominent in the nanoscale regime. We also demonstrate the method's simplicity and power with a three-dimensional simulation study of a quantum dot using a six band $\mathbf{k}\cdot\mathbf{p}$ Hamiltonian for holes as model.**

I. Introduction

In the rapidly evolving field of nanoelectronics one encounters problems that involve multiple interacting physical systems. One common scenario is that of the electronic system interacting with optical fields, static electrical and magnetic fields, lattice vibrations, and others. The electronic system itself has to be treated quantum mechanically due to the small length scales and quantum confinement. The other fields often require to be treated self-consistently with the electronic system.

When dealing with such problems two challenges arise: One is the high computational effort usually required for the analysis of such coupled systems. The expendable computational effort is limited by the availability and performance of computational hardware on one hand and by the scalability of numerical algorithms on the other. The other challenge one faces is the semantic effort required to numerically model multliple systems simultaneously. This challenge is addressed in this work.

II. Computational Methods

Most physical laws are laws of conservation. Conservativity, therefore, serves as a common basis for the numerical modeling in our simulation framework. The finite volume method (FVM) posesses the inherent property of conservativity and is therefore well-suited as a common discretization formalism for all problems ocurring in nanophysical devices.

A. Discretization

Traditional FVM codes are edge-based (see e.g. [1]); here, a mesh node (i) couples to its neighbors (j) via the edges of the mesh graph. Each edge stores a length d_{ij} and a coupling area A_{ij}, each node stores its Voronoi cell volume V_i, see Fig. 1. The projection of the field, i.e. the derivative of a quantity φ along an edge, is approximated by $(\varphi_j - \varphi_i)/d_{ij}$. Some

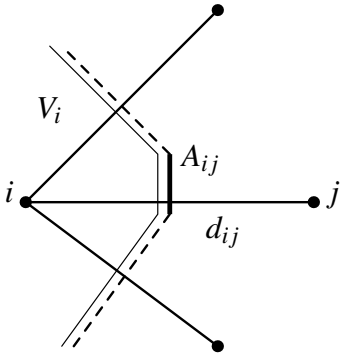

Fig. 1. Edge-based FVM discretization

material property (permittivity, effective mass, ...) relates the field to a flux density which is multpiplied by A_{ij} to obtain the partial flux leaving the cell. This approach has one major shortcoming: The field obtained by $(\varphi_j - \varphi_i)/d_{ij}$ is not the gradient of φ but only its projection along $\vec{e}_{ij}$ which implicitly assumes that the flux density caused by the field is parallel to $\vec{e}_{ij}$ as well. This restricts the discretization to isotropic media, i.e. ones with scalar field-flux relations.

Our FVM approach is element-based. Instead of looking at the neighbor nodes (j) of node i we look at its neighbor elements (l). Fig. 2 outlines this. The field is now calculated inside the element l in its vectorial form. For a simplex element (a triangle in two dimensions, a tetrahedron in three dimensions) the approximate gradient of a quantity φ is constant within the element and can be obtained by

$$\left[\vec{\nabla}\varphi\right]^l \approx \mathbf{Y}^l \begin{bmatrix} \varphi_j - \varphi_i \\ \varphi_k - \varphi_i \\ \vdots \end{bmatrix}, \quad \mathbf{Y}^l := \mathbf{U}^l \left((\mathbf{U}^l)^T \mathbf{U}\right)^{-1}, \qquad (1)$$

where $\mathbf{U} := [\vec{d}_{ij},\ \vec{d}_{ik},\ \ldots]$ is a matrix containing the edge vectors of the element with respect to node i as columns. The vectorial field may now be multiplied with a second order tensor to obtain the flux density. The dot product of the flux density with the coupling area vector $\vec{A}_{il}$ gives the partial flux leaving the cell.

978-1-61284-418-3/11/$26.00 © 2011 IEEE

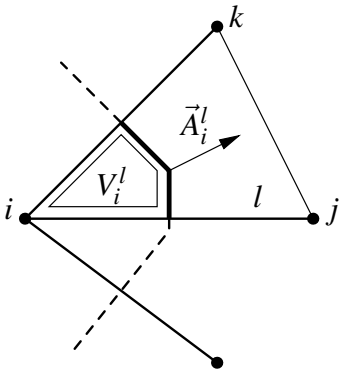

Fig. 2. Element-based FVM discretization

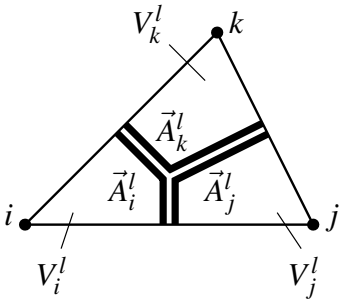

Fig. 3. The anatomy of an element

B. Assembly

In a realistic mesh the number of elements is several times greater than the number of nodes. To reduce the number of times a particular element has to be evaluated when building the system matrix the assembly is element-centric: A loop iterates over the elements of the simulated structure and has the partial fluxes between the element's vertices evaluated. These are then added to the appropriate elements of the system matrix.

This kind of assembly also allows the discretization of the problem's constitutive partial differential equations (PDE) to be broken down on a per-element basis. Continuous operators and operands can be directly translated into discrete ones which are represented by matrices. Tab. I shows how continuous vector-analytic operators (gradient and divergence) as well as continuous quantities are related to their discrete per-element representations as matrices. Operand matrices are diagonal and each diagonal entry corresponds to the operand's value at each of the element's vertices, hence for an n-dimensional simplex with $n_v = n+1$ vertices, the element operands are n_v-dimensional diagonal matrices. Operators in contrast are full matrices; A^l is a $n_v \times 3$ matrix and contains the area vectors of the coupling surfaces between the element's vertices (see Fig. 3) as rows; Z^l is a $3 \times n_v$ matrix and relates the values at the nodes to the gradient vector within the element. Second order operators (see Tab. II) and entire PDEs may be assembled by multiplying the corresponding matrices. This also allows the assembly of mixed derivatives such as $\partial^2/\partial x \partial y$ which are just a special case of an anisotropic

TABLE I
CONTINUOUS OPERATORS AND OPERANDS WITH THEIR DISCRETE COUNTERPARTS

	Continuous	Discrete
Gradient	$\vec{\nabla}$	$\mathbf{Z}^l = \left[-\mathbf{Y}^l[1\ 1\ \ldots]^T,\ \mathbf{Y}^l\right]$
Divergence	$\mathrm{d}V\mathrm{div}$	$\mathbf{A}^l = [\vec{A}_i^l,\ \vec{A}_j^l,\ \ldots]^T$
Control volume	$\mathrm{d}V$	$\mathbf{V}^l = \mathrm{diag}(V_i^l,\ V_j^l,\ \ldots)$
Scalar quantity q	$q(\vec{r})$	$\mathbf{q}^l = \mathrm{diag}(q_i,\ q_j,\ \ldots)$

TABLE II
COMMON ELEMENTS OF PDES IN THEIR DISCRETIZED FORM

	Continuous	Discrete
Laplacian	$\mathrm{d}V\nabla^2$	$\mathbf{A}^l\mathbf{Z}^l$
Anisotropic Laplacian	$\mathrm{d}V\vec{\nabla}\cdot\underline{\tau}\cdot\vec{\nabla}$	$\mathbf{A}^l\boldsymbol{\tau}^l\mathbf{Z}^l$
First order derivative	$\mathrm{d}V\vec{e}_k\cdot\vec{\nabla}$	$\mathbf{V}^l(\vec{e}_k[1\ 1\ \ldots])^T\mathbf{Z}^l$

Laplacian with $\underline{\tau} = \vec{e}_x \otimes \vec{e}_y$. A per-element $n_v \times n_v$ matrix obtained by a combination of the aforementioned matrices has its entries added to the appropriate entries in the system matrix, denoted by the global indices of the element's vertices.

Note that the number of columns in A^l and rows in Z^l is three regardless of the dimensionality of the elements (lines, triangles, or tetrahedra) meaning that models always operate in three-dimensional real space even if the simulation domain is one-dimensional. This has several benefits:

- It is useful when describing the influence of transversal asymetries, e.g. transversal electromagnetic field in a one-dimensional device.
- Tensors operating on three-dimensional vectors can be used in lower-dimensional models to conveniently express effects of substrate rotation.
- Mixed-dimensionality problems are possible, e.g. a graphene layer on a substrate, where carrier transport is two-dimensional but the electrostatics need a full three-dimensional treatment due to the influence of the substrate.

III. RESULTS AND DISCUSSION

The implementation of the presented scheme was realized within the Vienna Schrödinger-Poisson simulation framework (VSP) [2]. As an illustrative study for the method and its implementation we have chosen the problem of calculating the quantized hole states in a silicon quantum dot. From a six band $\mathbf{k}\cdot\mathbf{p}$ Hamiltonian the effective Hamiltonian for the quantum dot is obtained from which the quantized hole structure is calculated. The model Hamiltonian contains strong anisotropy as well as mixed derivatives which makes the model suitable as a test case for our simulation framework.

A. The Model Hamiltonian

The model Hamiltonian reads [3]

$$H_{6\times6} = H_{3\times3} \otimes \begin{bmatrix} 1 & 0 \\ 0 & 1 \end{bmatrix} + H_{\mathrm{so}} \tag{2}$$

with

$$H_{3\times3} = \begin{bmatrix} Lk_x^2 + Mk_{y,z}^2 & Nk_xk_y & Nk_xk_z \\ Nk_xk_y & Lk_y^2 + Mk_{x,z}^2 & Nk_yk_z \\ Nk_xk_z & Nk_yk_z & Lk_z^2 + Mk_{x,y}^2 \end{bmatrix} \quad (3)$$

and

$$H_{\mathrm{so}} = -\frac{E_{\mathrm{so}}}{3} \begin{bmatrix} 0 & \sigma_x\sigma_y & \sigma_x\sigma_z \\ \sigma_y\sigma_x & 0 & \sigma_y\sigma_z \\ \sigma_z\sigma_x & \sigma_z\sigma_y & 0 \end{bmatrix}. \quad (4)$$

The three-band paramters in (3) are $L = -6.53$, $M = -4.64$, and $N = -8.75$ in units of $\hbar^2/2m_e$ [4]; the split off energy E_{so} is 44 meV [5]. σ_ξ are the Pauli spin matrices.

By replacing $\vec{k} = k_x\vec{e}_x + k_y\vec{e}_y + k_z\vec{e}_z$ with $-i\vec{\nabla}$ one obtains the real space representation of the Hamiltonian. The real space representation is discretized in the following step. The eigenenergies and states of the dot are obtained by numerically solving the algebraic eigenvalue problem arising from the discretization and assembly procedure.

B. Meshing, Discretization, and Numerics

The simulated structure is a silicon quantum dot embedded in a SiO_2/Si_3N_4 matrix, a structure commonly found in photoluminescence experiments [6]. The dot has the geometric shape of a rhombicuboctahedron and measures 5 nm along its $\langle 100 \rangle$ axes. Its outline can be seen in Fig. 5. The structure was meshed using *TetGen*, a three-dimensional tetrahedral mesh generator [7]. The generated mesh was completely irregular and contained a few ten thousands of points. The irregularity of the mesh breaks the otherwise octahedral symmetry of the dot. This has the effect that states, which are perfectly degenerate in the continuum picture due to symmetry and would be also numerically degenerate if an orthoproduct grid was used, have their energies split slightly. The splitting was however found to be very low in our example (rel. err. $\approx 10^{-5}$). Thus the states can be considered *quasi-degenerate*. The mesh also contained about one percent of "bad tetrahedra", i.e. tetrahedra with ill-scaled aspect ratios. Some of these tetrahedra cause the matrix of the per-element Lapacian $\mathbf{L}^l = \mathbf{A}^l\mathbf{Z}^l$ to become indefinite which in turn causes non-vanishing (but small) imaginary parts in some of the system matrix eigenvalues.

The discretization of the Hamiltonian results in a straightforward translation of operators according to Tab. II. The diagonal elements of (3) are discretized analogous to

$$Lk_x^2 + Mk_{y,z}^2 \mapsto -\vec{\nabla} \cdot \begin{bmatrix} L & & \\ & M & \\ & & M \end{bmatrix} \cdot \vec{\nabla} \mapsto -\mathbf{A}^l \begin{bmatrix} L & & \\ & M & \\ & & M \end{bmatrix} \mathbf{Z}^l, \quad (5)$$

and the off-diagonal ones analogous to

$$Nk_xk_y \mapsto -\frac{1}{2}\vec{\nabla} \cdot \begin{bmatrix} N & & \\ & N & \\ & & \end{bmatrix} \cdot \vec{\nabla} \mapsto -\frac{1}{2}\mathbf{A}^l \begin{bmatrix} N & & \\ & N & \\ & & \end{bmatrix} \mathbf{Z}^l. \quad (6)$$

Closed (Dirichlet) boundary conditions were applied.

To save computational effort, only the three band Hamiltonian $H_{3\times3}$ was discretized and its eigenenergies and states were computed as a first step, thus excluding the effect of spin-orbit coupling. This part of calculation was done efficiently using the implicitly restarted Arnoldi method (IRAM) provided by ARPACK [8]. We exploited the sparsity of the system matrix in the matrix-vector multiplications and only a few physically relevant eigenpairs were computed. In the second step, the six band Hamiltonian was expanded using the $H_{3\times3}$ states from the previous step as basis. The resulting dense (but small) eigenvalue problem was solved using direct methods (LAPACK [9]). Spin-orbit coupling mainly causes splitting among (quasi-)degenerate states. The expansion therefore gives a good approximation even for a very small set of basis states.

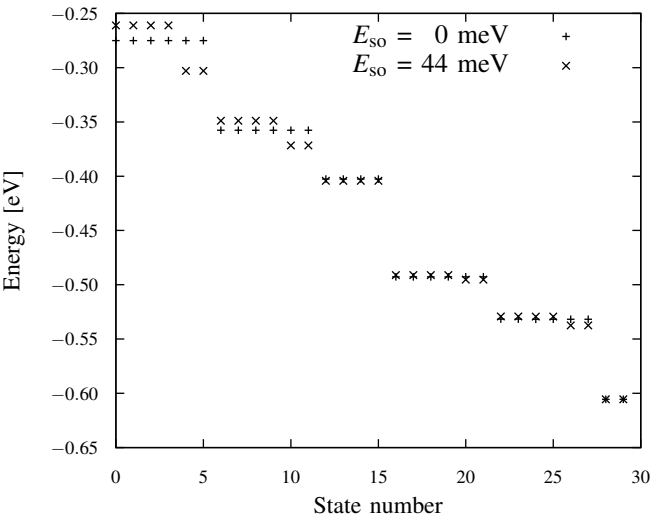

Fig. 4. Quantum dot energies with (×) and without (+) spin-orbit coupling; most states are six fold (quasi-)degenerate; spin-orbit coupling breaks the six fold degeneracies into two and four fold ones

C. Numerical Results

Fig. 4 shows the eigenenergies of the simulated quantum dot. Most of the states are (quasi-)degenerate due to the symmetric structure geometry. The most common degeneracy multiplicity is six which corresponds to the number of bands (three) times spin polarizations (two). Multiplicities other than six are due to non-parabolicity effects. Spin-orbit coupling partially lifts the six fold degeneracies and breaks them into doublets and quadruplets.

Fig. 5 shows the densities corresponding to each cluster of degenerate states. The density distributions develop very unusual shapes due to the non-parabolicity of the Hamiltonian. The densities are almost unaffected by spin-orbit coupling; the densities with and without spin-orbit coupling are visually indistinguishable.

IV. Conclusions

A finite volume discretization method for the simulation of nanoelectronic devices was presented. The method's capabilities were demonstrated using a three-dimensional analysis of the closed boundary $\mathbf{k} \cdot \mathbf{p}$ Schrödinger equation. Similar work was done in [10] using finite differences and in [11]

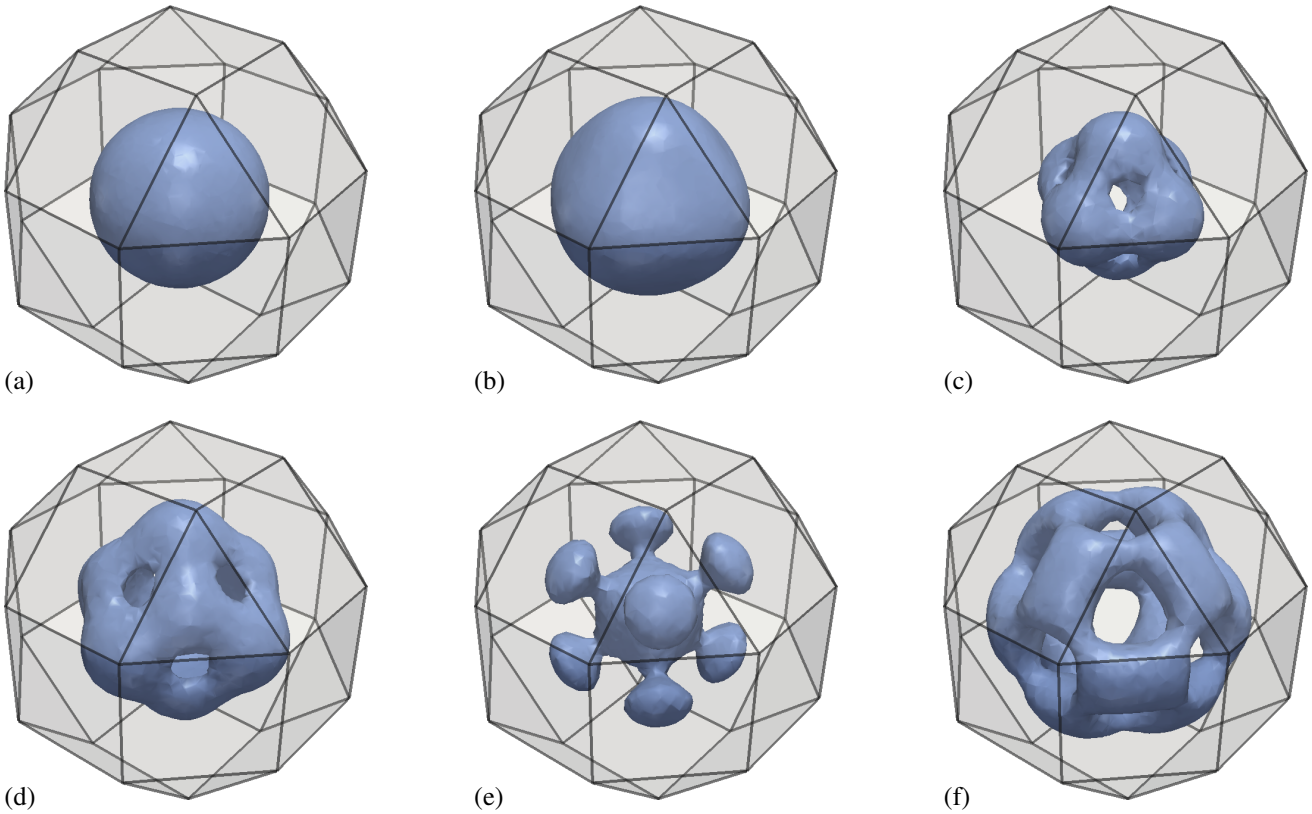

Fig. 5. Contours of densities corresponding to quantized hole states in a silicon quantum dot; densities of (quasi-)degenerate states are summed in this figure; (a) states 0 through 5, (b) states 6 through 11, (c) states 12 through 15, (d) states 16 through 21, (e) states 22 through 27, (f) states 28 and 29

using finite elements. To our knowledge, this is the first implementation of a $\mathbf{k} \cdot \mathbf{p}$ Schrödinger solver using finite volumes and a three-dimensional irregular mesh. Finite volumes are a widespread approach in device simulation due to the physical basis of the discretization scheme (laws of conservation). This allows a consistent integration of classical and advanced nanodevice simulation, where the inclusion of anisotropy and strain and orientation effects opens new opportunities in the device design and engineering process.

V. Acknowledgement

This work has been supported by the Austrian Science Fund, special research program IR-ON (F2509).

References

[1] K. M. Kramer and W. N. G. Hitchon, *Semiconductor Devices*, J. Czerwinski, Ed. Prentice Hall, 1997.

[2] M. Karner *et al.*, "A multi-purpose Schrödinger-Poisson Solver for TCAD applications," *Journal of Computational Electronics*, vol. 6, no. 1, pp. 179–182, Sep. 2007.

[3] T. Manku and A. Nathan, "Valence energy-band structure for strained group-IV semiconductors," *Journal of Applied Physics*, vol. 73, no. 3, pp. 1205–1213, 1993.

[4] Frank L. Madarasz *et al.*, "Effective masses for nonparabolic bands in p-type silicon," *Journal of Applied Physics*, vol. 52, no. 7, pp. 4646–4648, 1981.

[5] M. Levinstein *et al.*, "Handbook Series on Semiconductor Parameters vol 1, 2," *World Scientific, London*, vol. 1999, p. 191, 1996.

[6] Z. T. Kang *et al.*, "Synthesis of silicon quantum dot buried SiO_2 films with controlled luminescent properties for solid-state lighting," *Nanotechnology*, vol. 17, no. 17, p. 4477, 2006.

[7] H. Si. (2011). [Online]. Available: http://tetgen.berlios.de/

[8] R. Lehoucq *et al.*, *ARPACK Users' Guide: Solution of Large-Scale Eigenvalue Problems with Implicitly Restarted Arnoldi Methods*, 1998.

[9] E. Anderson *et al.*, "LAPACK: a portable linear algebra library for high-performance computers," in *Proceedings of the 1990 ACM/IEEE conference on Supercomputing*, ser. Supercomputing '90. Los Alamitos, CA, USA: IEEE Computer Society Press, 1990, pp. 2–11.

[10] A. Trellakis *et al.*, "The 3D nanometer device project *nextnano*: Concepts, methods, results," *Journal of Computational Electronics*, vol. 5, pp. 285–289, 2006.

[11] R. Veprek *et al.*, "Reliable k · p band structure calculation for nanostructures using finite elements," *Journal of Computational Electronics*, vol. 7, pp. 521–529, 2008.